International Research Journal of Pharmacy and Medical Sciences
ISSN (Online): 2581-3277

Synthesis and Characterization SnO_2/ZnO Ratio 1:1.25 Nanocomposite by Electrochemical Technique and Evaluated by Degradation of Alizarin Red S dye

Hayder Khudhair Khattar[1*]
[1]College of Health and Medical Techniques, Al-Furat Al-Awsat Technical University, 54001 an-Najaf, Iraq
*Corresponding author, email: haider.khattarckm11@atu.edu.iq

Abstract**—***By using electrochemical precipitation method was prepared a SnO_2/ZnO nanocomposite with a ratio of 1:1.25 a, and its structu ral and surface characteristic were studied utilize XRD, FTIR, FESEM, HRTEM, and EDX techniques. Which confirmed crystallographic and structural analyses the construction of a homogeneous and well-crystalline nanocomposite sizes of about 19 nm and a symmetric elemental distribution. The morphology images explain interparticle adhesion, which raise highly efficient electron–hole pair separation. The execution of the nanocomposite as a photocatalyst for the degradation of alizarin red S (ARS) dye was estimated in a home-made photoreactor used lampe 250 W, UV illumination. The experience involved preparing the dye solution, modify the pH and catalyst concentration, and con stantly stirring to reach adsorption equilibrium with absence of UV rays %PDE 16.21. The effects of operating variables such as dye concentrat ion, catalyst dosage, and pH on the photodegradation efficiency were studied. The results demonstrated high dye removal efficiency (>86%) under optimized conditions (dye concentration 20 ppm, catalyst dosage 0.5 g, and pH ≈ 9 , temperatur K338). revealed analyses of Kinetic and thermodynamic, low activation energy (Ea = 8.95 kJ/mol-1), signal that the photocatalytic reaction is largely temperature independent. The positive enthalpy and free energy values (ΔH* and ΔG*) specified that the reaction is endothermic and nonspontaneous beneath the experimental c onditions, while the negative entropy (ΔS* < 0) tick that the transition state is more systematic. The high catalytic efficiency of the nanocomposite is refer to the efficient generation of reactive species such as hydroxyl radicals (•OH) and superoxide anions (O_2^-) on the surface of the composite, which participate to the decomposition of organic pollutants into modest products such as CO_2 and H_2O, the results proved tha t the reaction behaves as a pseudo-first-order reaction, Langmuir-Hinshelwood model. This project explain that the SnO_2/ZnO (1:1.25) nanocomposite system is functional and promising for industrial and environmental wastewater treatment applications.*

Keywords**—** *Electrochemical, SnO_2/ZnO ratio 1:1.25 Nanocomposite, Photodegradation.*

I. INTRODUCTION

Dangerous organic waste is one of the most prominent environmental problems facing various industrial sectors, due to its great negative impact on the environment and human health. To reduce these pollutants, many processing techniques have been developed, including oxidation processes that aim to dismantle organic pollutants and convert them into simple, harmless compounds [1-4]. In the field of heterogeneous optical stimulation, mineral oxides such as TiO_2 and ZnO have emerged as promising materials that have their high ability to dismantle organic pollutants, especially fabric dyes, while reducing emissions or secondary pollutants to the lowest possible [5-7]. ZnO is one of the most used materials in UV-UV. Thanks to its wide range of about 3.2 electron volts, along with its low cost and high chemical stability, it is an ideal choice in dismantling organic pollutants and treating environmental waste [8-12]. When the surface of the particle is exposed to light, electrons are transmitted from the equal range to the delivery range, resulting in the formation of pairs of electrons and gaps (e^-/h^+). These husbands stimulate the reactions of oxidation and reduction on the surface of the material, which leads to the disintegration of organic pollutants and converts them into simpler compounds such as carbon dioxide and water. Nevertheless, many of the photogenerated electron-hole pairs are in a single-phase photocatalyst, in a large reinstallation, or on the surface of the particles. However, many photogenerated electron-hole pairs in single-phase photocatalysts undergo significant recombination or occur on the particle surface. Many efforts are being made to reduce this recombination rate by incorporating dopants with external sources or by coupling with semiconductor oxides that have a suitable band gap to introduce heterojunctions. Considerable heterogeneous functional oxides, like CuO and ZnO, possess high photocatalytic efficiency due to their ability to absorb light and result electron-hole pairs effectively, which elevate photocatalytic reactions at their surfaces. The formation of a heterojunction among these two oxides also contribute in amended charge division and reduced recombination, thus rising photocatalytic fulfillment, especially in the therapy of organic pollutants [13,14]. ZnO and TiO_2 [15-17], ZnO and CdS [18], etc. One candidate to reduce the recombination rate of the ZnO photocatalyst is by compositing with the SnO_2 phase [19-22]. SnO_2 works as an electron, while the holes tend to move from the equivalence of SnO_2 towards ZnO, which leads to an effective separation of electron-hole pairs. Previous studies have shown that the inclusive ratio between Zn and Sn in the ZnO-SnO compound greatly affects its properties [23-25]. These systems have been widely studied, but the effect of the basic material pussy is rarely mentioned. The structure of the ZnO-SnO_2 nanopotype can be prepared using several analytical chemical methods, such as the electrochemical method [26]. and microemulsion methods [27]. Sol-gel: This wet chemical technique include converting precursors to a gel, which is then dehydrated and sintered to compose the wanted

Hayder Khudhair Khattar, "Synthesis and Characterization SnO2/ZnO Ratio 1:1.25 Nanocomposite by Electrochemical Technique and Evaluated by Degradation of Alizarin Red S dye," *International Research Journal of Pharmacy and Medical Sciences (IRJPMS)*, Volume 9, Issue 1, pp. 6-16, 2025.

nanomaterial. While relatively simple, it can demand long processing times and the employ of surfactants or stabilizers [28]. Laser ablation: this technique utilize a laser to steam a target material, creating nanoparticles in a liquid medium. It can produce high-quality nanoparticles; however, the tools can be expensive, and scaling up manufacture can be challenging [29]. Hydrothermal process, employ high-pressure and high-temperature water for chemical reactions, can be effective for synthesizing ZnO/SnO_2 materials but often require complex setups and specific conditions. The process consist on the solubility of reactants in water beneath large temperatures and pressures within a closed vessel [30]. The electrochemical method is the preferred method, which is a simple, reliable, and inexpensive method. In this article, synthesized SnO_2/ZnO nanocomposites enhance the photocatalytic activity of tin, observed as the wide band gap of SnO_2 decreased from 3.6 eV to 2.916 eV in SnO_2/ZnO [31]. In this work, the ZnO/SnO_2 nanocomposite powder was prepared with a molten (1:1) percentage using the chemical method, and its performance was evaluated in the optical decomposition of the Alizarin Red dye. The FESEM electronic microscope was also used to study the morphology and microstructure of the thin films. This study focuses on the synthesis of SnO_2/ZnO nanocomposite using an effective and surfactant-free electrochemical method. The research aims to take advantage of the priority of electrical expression, such as the exact control of the thickness of the film, uniformity, and formation, to produce these nanoparticles. The study will investigate the structural and optical properties of the synthesized nanocomposite, with the aim of exploring their potential applications in electronics, antibacterial and sensor technologies, and photodegradation properties. The advantages of electrogeneration include its low cost, low energy consumption, environmentally friendly nature, reduced material waste, and the ability to produce thin films at low temperatures. The nanocomposite formation process and fundamental properties can be controlled by adjusting the applied potential [32]. However, the main limitation is that this technique is generally unsuitable for large-scale production. Therefore, the deposition process should be improved to achieve ideal conditions. The properties of the obtained nanocomposite have been distinguished by the techniques UV-Vis, FTIR, XRD, FESEM, EDX, and HRTEM.

II. Material and Method

Prepare a 1:1.25 SnO_2/ZnO nanocomposite using a 200 ml glass cell. The system includes a positive electrode (anode) made of a 4 cm tin plate (99% purity Aldrich) and a zinc electrode of the same area (99% purity Aldrich). The negative electrode (cathode) is made of 4 cm graphite. The electrodes are washed with ethanol and then deionized water to remove any suspended organic matter. Add approximately 1 gram of a strong electrolyte, such as KCl. Add 20 ml of a solution containing 1 gram per 100 ml of stabilizer (polyvinyl alcohol, PVA). Add 135 ml of deionized water and a zinc foil (4 cm × 2 cm × 0.25 mm) for use in one test, plus an tin foil (4 cm × 2 cm × 0.25 mm) for the other tests. The electrodes (anode and cathode) are placed facing each other in the electrolyte solution, each 2 cm deep. The electrolyte is equipped with a device that supplies a current of up to 5,000 milliamps (mA) and a maximum of 30 volts (V). This device serves as a magnetic stirrer to stir the mixtures. The electrolyte is operated for one hour at a temperature of 40 to 50°C. The precipitates are then centrifuged and washed three times with deionized water and ethanol. The precipitates are dried at 60°C for one hour, then calcined in an oven at 200°C for two hours. A certain weight of ZnO from the first experiment 0.70 g was added to the certain weight of the electrolytic cell. In the second experiment, 0.70 g of SnO_2 were added to obtain SnO_2 /ZnO composites using a 1:1.25 ratio, as shown in Table 1. The process needs to control the size of nanoparticles by changing the size of the electrodes. This is mostly true for the zinc anode, which has an area of 4 cm^2 and a total area of 32 cm^2, and the graphite cathode, which has the same area. In the second experiment, tin electrode were prepared to the required dimensions before the operation and in the same space. 135 mL of deionized water with 25 mL of 2-propanol (C_3H_8O) , used to increase the reaction temperature and suppress agglomeration, ensuring homogeneity of the solution. 20 ml of PVA with 20 ml of KOH , used as electrolyte. EDX analysis indicated that the atomic ratio of SnO_2/Al_2O_3 was 1:1.25.

TABLE 1. Demonstrate , measurements , EDX and empirical data

No. Exp.	Chemicals		EDX
	KCL (99% Thomas ,Indi)	0.5 g/100ml	Exp: 1+2 ZnO/Al_2O_3 w/w %= 0.70g/0.70g Zn =32.1 Sn= 26.1 Atomic % ratio =(1:1.25) O= 41.9
	KOH (99% Thomas ,Indi)	5g/100 ml We take 20 ml	
	PVA (CDH-India)	1g/100 ml We take 20 ml	
	Deionizedwater	0.7 µS/cm 135 ml	
	2-propanol (C_3H_8O) M.Wt:60.10	25 ml	
	pH	10-12	
	Temperature	40-50 ^oC	
	Current density	500 mA/m^2	
1	Sn (4cm^2) Anode area	32 cm^2	
	Graphite cathode	32 cm^2	
	Current density	1.6 -1.8 A	
	Voltage/time	9-12 V/60 (min)	
2	Al (4cm^2) Anode area	32 cm^2	
	Graphite cathode	32 cm^2	
	Current density	1.6-1.9 A	
	Voltage/time	9-12 V/60 (min)	

III. Results and Discussion

UV-visible analysis

The ultraviolet–visible (UV-Vis) spectrum of the SnO_2/ZnO composite in the range of 400–600 nm showed that the prepared nanoparticles exhibited significant photoactivity under visible light irradiation The band gap of SnO_2/ZnO was calculated using Tauc′s plot Fig.1. For a semiconductor sample, it is possible to determine the optical absorption near the band edge by the equation, $\alpha hv=A(hv-Eg)^{n/2}$ where α, h, v, Eg and A are absorption coefficients, Planks constant, radiation frequency, band gap and good stability. The n value determines the nature of the transition in a semiconductor,

Hayder Khudhair Khattar, "Synthesis and Characterization SnO2/ZnO Ratio 1:1.25 Nanocomposite by Electrochemical Technique and Evaluated by Degradation of Alizarin Red S dye," *International Research Journal of Pharmacy and Medical Sciences (IRJPMS)*, Volume 9, Issue 1, pp. 6-16, 2025.

with n=1 for the direct transition and n=4 for the indirect transition. To accurately determine the energy gap, the relationship between $(\alpha h\nu)^{1/2}$ and hv, known as the Tauc diagram, was drawn [33]. By analyzing the optical absorption spectra, it was found that the SnO_2/ZnO nanoparticles had a maximum absorption peak at 484 nm, and the band gap was calculated from the Tauc diagram to be 2.8 eV.

Infrared Spectroscopy (FT-IR) Analysis:

Figure 2 exhibit the infrared spectrum of SnO_2/ZnO nanocomposite. This analysis objective to recognize the functional groups and chemical bonds existent in the compound structure. The spectrum expose characteristic absorption peaks signal Sn-O and Zn-O bond vibrations, confirming the formulation of tin and zinc oxides within the nanostructure of the compound. Additional weak peaks may also show, resulting from the existence of $^{-}$OH groups on the surface, which are commonly associated with adsorbed water molecules or surface defects in the nanoparticles. The IR spectra signalize that the absorptions at 3446 cm^{-1} are obviously related to the subsistence of hydroxyl groups of water molecules [18] on the external surface of SnO_2 nanoparticles. The peaks at 1172 and 856 cm^{-1} correspond to the bending and stretching vibration of Sn-O. The peak at 1439 cm^{-1} indicates the formation of ZnO; the characteristic of the FTIR peak appears in Table 2. [19,20].

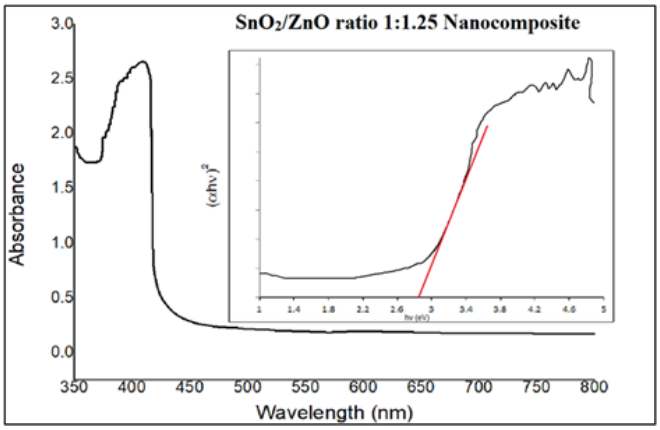

Figure 1. UV.vis spectra of the SnO_2/ZnO ratio 1:1.25 Nanocomposite and and Tauc's plots Eg = 2.8 eV.

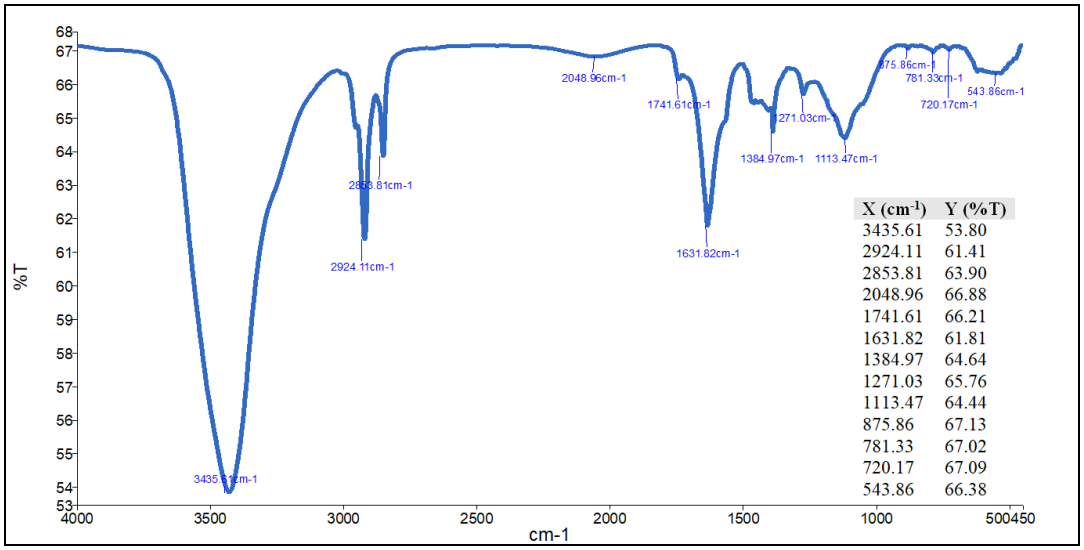

Figure 2. Distinguishing peaks of FTIR spectrum for SnO_2/ZnO, ratio (1:1.25) nanocomposites

TABLE 2. Characteristic the peaks in the FTIR spectrum and the functional groups of SnO_2/ZnO, ratio (1:1.25) nanocomposites

Wave number (cm^{-1})	Effective group/vibration type	Interpretation	Ref.
3400 – 3450	O–H stretching vibration	It indicates the presence of hydroxyl groups (–OH) or water adsorbed on the surface of the particles.	[37]
1600 – 1630	O–H bending vibration	Bound to absorbed water or hydroxyl groups	[38]
1000 – 1100	M–O–M vibration (metal–oxygen–metal)	It indicates the formation of bonds between Zn–O–Sn in the nanostructure of the compound.	[39]
500 – 700	Zn–O and Sn–O vibration	It confirms the presence of zinc oxides (ZnO) and tin oxides (SnO_2) in the nanocomposite.	[40]

XRD diagnosis

The XRD pattern illustration in Figure 3 of the fabricated SnO_2/ZnO ratio of 1:1.25 nanocomposite from which it was organized that the diffraction peaks at 2θ account for 31.81°, 34.62°, 36.19°, 47.49°, 56.61°, 62.85°, 66.39°, 67.95°, and 69.13° correspond well with the (100), (002), (101), (102), (110), (103), (200), (112), and (201) planes of the hexagonal wurtzite structure of ZnO, respectively (JCPDS 36-1451) [41]. Also, the diffraction peaks at 2θ values of 26.64°, 33.82°, 37.89°, 51.76°, 54.71°, 64.76°, and 78.73° correspond well with the (110), (101), (200), (211), (220), (112), and (321) planes of tetragonal SnO_2, respectively (JCPDS 41-1445) [42].

Hayder Khudhair Khattar, "Synthesis and Characterization SnO2/ZnO Ratio 1:1.25 Nanocomposite by Electrochemical Technique and Evaluated by Degradation of Alizarin Red S dye," *International Research Journal of Pharmacy and Medical Sciences (IRJPMS)*, Volume 9, Issue 1, pp. 6-16, 2025.

So, the apparition of the lattice plane conforming to both the ZnO and SnO_2 implies the consistency of the SnO_2/ZnO nanocomposite [43]. Likewise, no impurity peaks were spotted in any of the XRD patterns. Further, from the diffraction peak of the XRD data, the average crystallite size was calculated using the Debye-Scherrer equation [44]: $D=0.9\lambda /\beta \cos\theta$. Here, D is taken as the crystallite size in nm, λ is the diffraction wavelength in A, β is the FWHM in radians, θ is the diffraction angle in degrees (°), and K is a constant, which is also called the shape factor, and its value is close to unity [45]. The crystallite size average of the invented SnO_2/ZnO nanocomposite was calculated using the overhead equation and found to be 19.12 nm. This shows that the average crystallite size of the invented SnO_2/ZnO nanocomposite was in the range of the average particle size measured from its TEM image. Since the XRD data of the fabricated SnO_2/ZnO nanocomposite was in good agreement with the TEM results, it further confirmed the formation of the SnO_2/ZnO nanocomposite. Bragg diffraction peaks are shown in table 3.

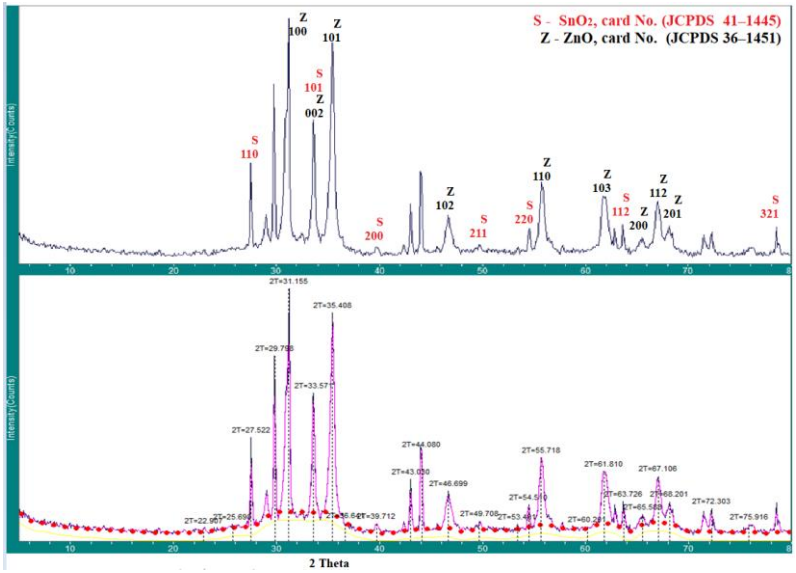

Figure 3. XRD patterns of SnO_2/ZnO ratio 1:1.25 Nanocomposite ; at 10-70° 2θ range.

TABLE 3. XRD difference of the different Bragg diffraction peaks of SnO_2/ZnO, ratio 1:1.25 Nanocomposite. crystal size 19.12 nm

2-Theta	d(nm)	BG	Height	I%	Area	I%	FWHM	crystal size (nm)
22.907	0.38791	0	65	5.3	773	11.8	1.011	8
25.698	0.34637	22	62	5	767	11.8	1.052	8
27.522	0.32382	28	517	42	1784	27.3	0.293	32
29.798	0.29959	100	878	71.4	1834	28.1	0.178	61
31.155	0.28684	105	1230	100	5438	83.3	0.376	25
33.571	0.26673	103	676	55	2748	42.1	0.346	27
35.408	0.2533	94	1112	90.4	6525	100	0.499	18
36.641	0.24505	51	40	3.3	444	6.8	0.944	9
39.712	0.22678	0	86	7	754	11.6	0.745	12
43.03	0.21003	9	315	25.6	1039	15.9	0.28	35
44.08	0.20527	13	456	37.1	1952	29.9	0.364	26
46.699	0.19435	20	241	19.6	2230	34.2	0.787	12
49.708	0.18326	12	88	7.2	1107	17	1.069	9
53.401	0.17143	14	71	5.8	321	4.9	0.384	26
54.51	0.1682	27	162	13.2	830	12.7	0.435	23
55.718	0.16484	35	402	32.7	3230	49.5	0.683	14
60.201	0.15359	17	53	4.3	519	8	0.832	12
61.81	0.14997	44	320	26	3219	49.3	0.855	12
63.726	0.14592	11	194	15.8	983	15.1	0.431	24
65.588	0.14222	40	97	7.9	1063	16.3	0.931	11
67.106	0.13937	50	289	23.5	2237	34.3	0.658	16
68.201	0.13739	43	161	13.1	1337	20.5	0.706	15
72.303	0.13057	1	166	13.5	1364	20.9	0.698	15
75.916	0.12523	0	83	6.7	1150	17.6	1.178	9

Surface morphology and elemental Composition of SnO_2/ZnO, (1:1.25) nanocomposite using FESEM, EDX and HRTEM

This portion of the analysis target to survey the surface morphology and elemental composition of the SnO_2/ZnO nanocomposite with a ratio of (1:1.25) by utilize three integrated techniques: Field-emission scanning electron microscopy (FESEM), images exhibit that the nanoparticles possess a homogeneous surface and a smooth, consolidated

Hayder Khudhair Khattar, "Synthesis and Characterization SnO2/ZnO Ratio 1:1.25 Nanocomposite by Electrochemical Technique and Evaluated by Degradation of Alizarin Red S dye," *International Research Journal of Pharmacy and Medical Sciences (IRJPMS)*, Volume 9, Issue 1, pp. 6-16, 2025.

structure with a good particle size division. It can also be seen that the particles arrange a spherical or rod-shaped shape, carefully interconnected, signalize good interpenetration between the ZnO and SnO_2 components as in Figur 4. The size of the nanoparticles is approx (a, b, c and d) depressed and high magnification FESEM images scal 45.68 - 62.03 nm and (c , d) HRTEM scal 40 , 20 nm. High-resolution transmission electron microscopy (HRTEM), images reveal that the nanocomposite have distinct crystalline structures with lattice border matching the crystal planes of ZnO and SnO_2, confirming the consistence of a heterostructured nanocomposite[46]. This structural correlation enhances the activity of electron transfer within the composite, a key factor in meliorative the photocatalytic properties. Energy Dispersive X-ray (EDX) Analysis, revealed the existence of only the major elements zinc (Zn=32.1), tin (Sn=26.1), and oxygen (O=41.9) atomic %, without impurities or strange elements, confirming the purity of the nanocomposite as in Figur 4 (a). The analysis also showed that the atomic ratio was approximately regular with the preparative ratio (1:1.25), signal a homogeneous elemental distribution in the sample show in firur 5. (b,c,d, and e) maping distribution of the items. The nanoparticles are tightly bound, contributing to the efficient separation of electron–hole pairs through photocatalysis. The size of the nanoparticles obtained from the HRTEM measurements was close to that obtained from the XRD measurements, with a value of about ±6[47].

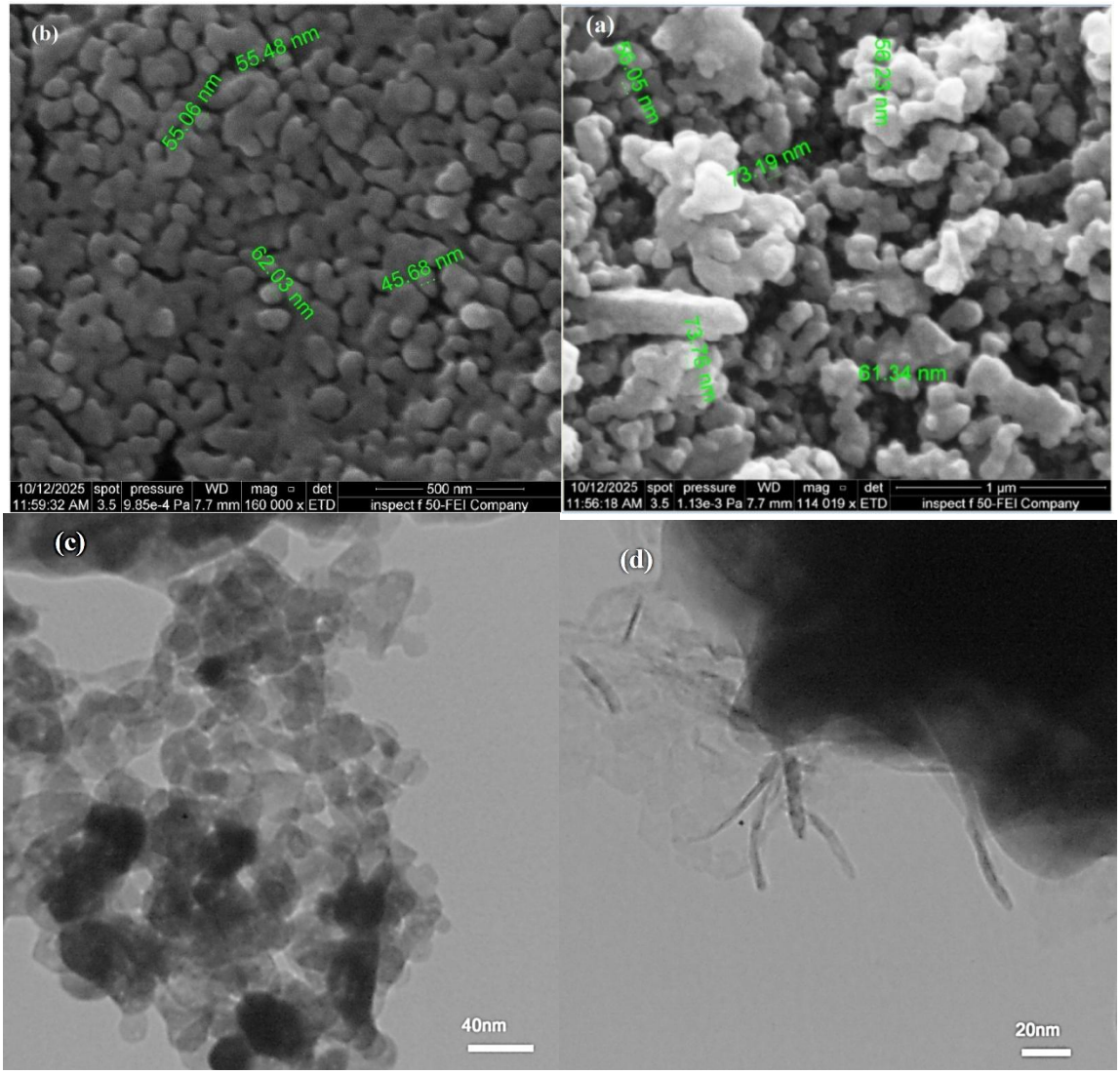

Figure 4. Structural and compositional analysis of the prepared SnO_2/ZnO ratio (1:1.25) nanocomposites. (a,b and c) Low and high magnification FESEM images scal 45.68 -62.03 nm and (c , d) HRTEM scal 40 , 20 nm.

Hayder Khudhair Khattar, "Synthesis and Characterization SnO2/ZnO Ratio 1:1.25 Nanocomposite by Electrochemical Technique and Evaluated by Degradation of Alizarin Red S dye," *International Research Journal of Pharmacy and Medical Sciences (IRJPMS)*, Volume 9, Issue 1, pp. 6-16, 2025.

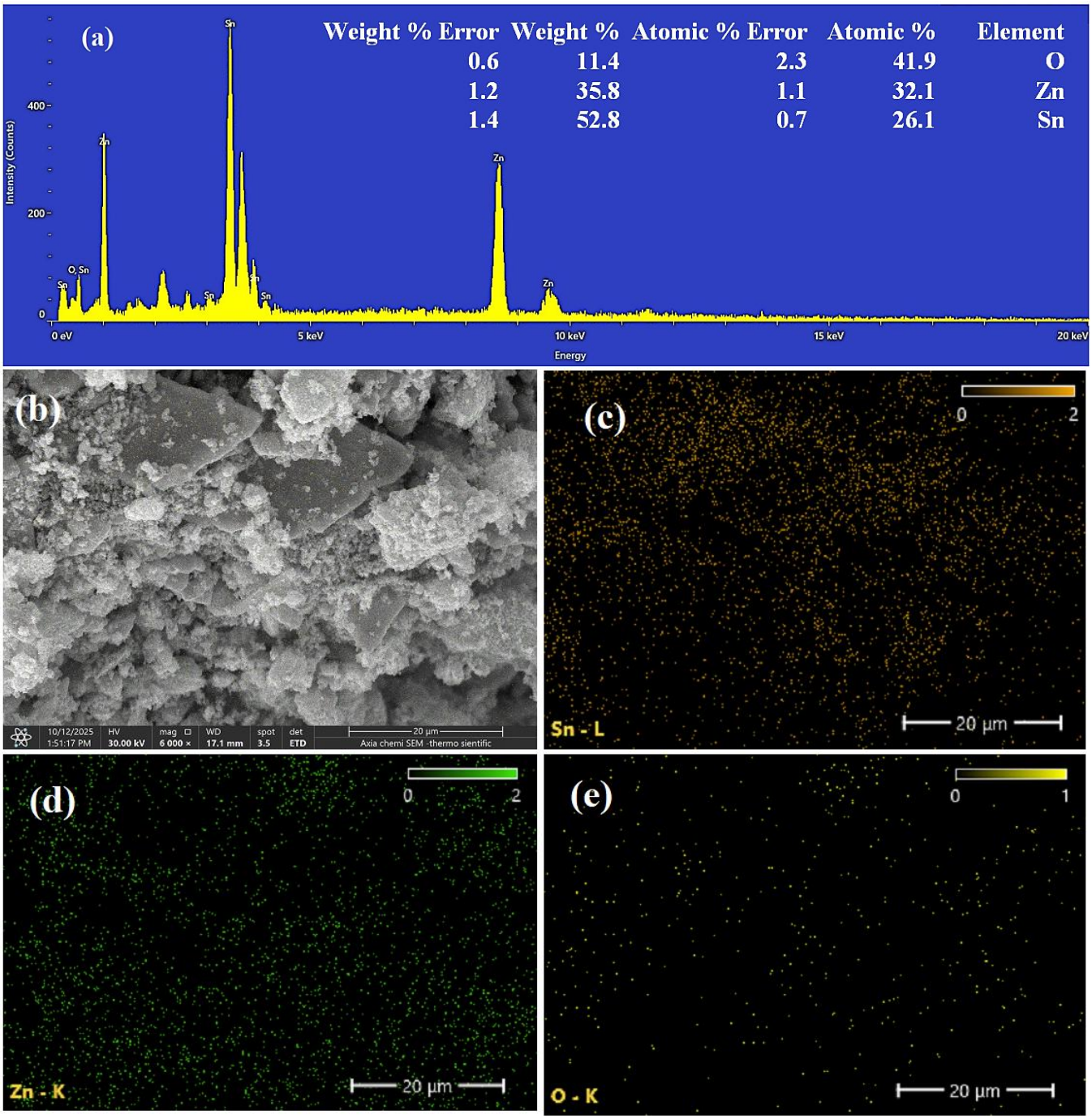

Figur 5. Compilation SnO_2/ZnO, ratio (1:1.25) nanocomposites (a) image shows the distribution of the elements, (Zn =32.1, Sn=26.1, O=41.9) Atomic % , (b,c,d, and e) maping distribution of the items

Alizarin red S Dye Description

Alizarin red S (ARS) (1,2-dihydroxy-9,10-anthraquinone sulfonic acid sodium salt; ARS; Mordant Red 3), molar mass=342.253 g/mol, maximum wavelength 470 nm [48], a water-soluble anthraquinone dye, has been exceedingly used in the textile industry since ancient times, and its uncontrolled release disturbs the ecosystem and poses a direct threat to both man and animals [49]. Therefore, an effective photocatalyst is needed for the efficient degradation of this hurtful dye, and an effective photooxidation of ARS is carried out utilizing the heterosystem SnO_2/ZnO ratio (1:1.25) nanocomposites. The optimization of physical parameters is similar to the initial ARS concentration, catalyst dose, initial pH, and chemical structure of Alizarin Red S, as in Figure 6.

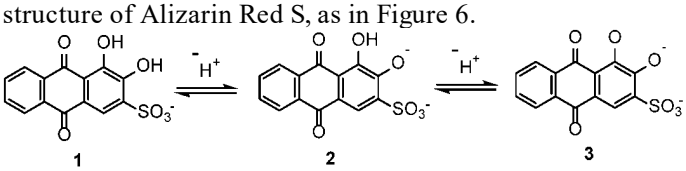

Figure 6. Chemical structure of Alizarin Red S (1) and its ionized structures (2 and 3) [50].

Hayder Khudhair Khattar, "Synthesis and Characterization SnO2/ZnO Ratio 1:1.25 Nanocomposite by Electrochemical Technique and Evaluated by Degradation of Alizarin Red S dye," *International Research Journal of Pharmacy and Medical Sciences (IRJPMS)*, Volume 9, Issue 1, pp. 6-16, 2025.

Photocatalysis activity:

The photocatalysis process is carried out using a homemade photocatalytic reactor. This unit is an aluminum box with wooden walls inside that help retain light and prevent light scattering. The photocatalytic reactor is also equipped with a medium-pressure mercury halogen lamp, MH-250W/640 E40 CLU1SL/12, from the German company Philips. A 250 W coverless is used to focus light vertically onto the solution. The prepared solutions were placed in a glass beaker. Leave a distance of 15 cm between the X-ray source lamp and the cup, and a magnetic stirrer is used for mixing. Photocatalytic analysis was complete on SnO_2/ZnO 1:1.25 nanocomposites as a catalyst for the elimination of ARS dye in a photocatalytic system at concentrations of 20-100 ppm. The solution was prepared by diluting a stock solution of 1000 ppm of ARS dye (99%, CDH India). The pH was controlled using 0.1 M NaOH or HCl. A 100 mL volume of ARS solution was placed inside the container, stored under continuous stirring and UV light, and dye adsorption occurred within 60 minutes without light. The photodegradation experiment was carried out continuously for 220 minutes. The results indicated that the structure of nanocomposites with a ratio of SnO_2/ZnO (1:1.25) has catalytic activity in isolation from light-darkening reactions, where the catalyst suffers from an adsorption process of the dye and forms a single layer of physical adsorption, and a slight disappearance of the dye is observed. Effectiveness of the adsorption dark reaction for the nanocomposite (PDE = 16.21, k = 0.43×10^{-4} sec^{-1}) shown in Figure 9. On the other hand, the dye irradiation process takes place in isolation from the catalyst, where the disappearance of the dye is observed without exaggeration due to the absence of the electronic transfer process provided by the catalyst as a result of the formation of an electron hole pair [51]. The result was the effectiveness of photocatalysis in the absence of the catalyst (PDE = 28.22%, k = 0.79×10^{-4} sec^{-1}) Observations indicate that the concentration of ARS changes linearly with extension of the irradiation time, suggesting the decomposition of ARS [52]. Thus, further exams were performed on the nanocomposite system. The effect of pH, catalyst dose, and ARS concentration on photosynthetic activity was studied.

Effect of pH

pH is a significant operating constant in wastewater treatment. When the dye is partially ionized, the electrostatic interactions occurring between the SnO_2/ZnO ratio (1:1.25) nanocomposites and the dye are taken into account, which depend on the pH of the solution, the zero charge point (PZC) of the adsorbent, and the pKa of the dye. The photodegradation produced under various pH values for dye is exhibited in Figure 7. These results showed that photochemical decolorization is best in alkaline solutions. It can be assumed that the degradation rate residue is almost like in the pH range between 9 PDE (82%) k=2.91×10^{-4} sec^{-1} and 12 PDE (80.5%) k=2.61×10^{-4} sec^{-1}.

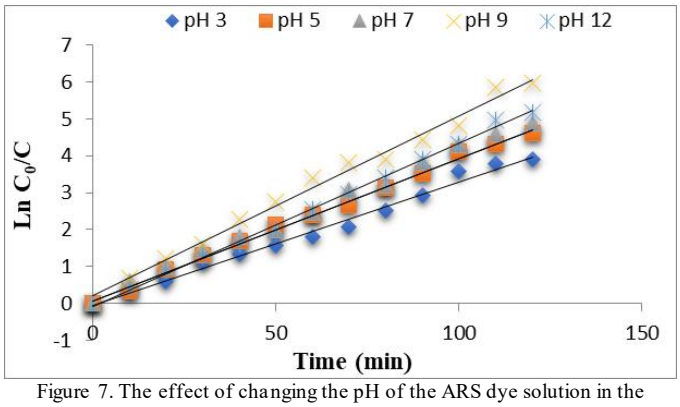

Figure 7. The effect of changing the pH of the ARS dye solution in the presence of the catalyst

Effect of catalyst dosage

The effect of catalyst dosage (0.1, 0.3, 0.5, 0.7, 0.9, 1 g) on the photoactivity of the SnO_2/ZnO ratio (1:1.25) nanocomposites is shown in Figure 8. As anticipated, the activity excess with increasing catalyst dose and the better photodegradation of ARS (84.9%) is acquired with a catalyst dose of 0.5 g and rate constant k=3.10×10^{-4}. This is simply due to the increasing number of photocatalytic sites and higher reception surface for incident photons [53]. The optical efficiency reduces as more powder is added due to saturation of photocatalytic sites, shading effects, and light scattering.

Influence of the initial ARS concentration

The influence of initial ARS concentration on the photodegradation rate is shown in Figure 9. The generality of the degradation happens at the irradiated surface (reaction region), where the light intensity is extremely higher than in the lower irradiated area (background region). Thus, for high ARS concentrations, the degradation in the minimally irradiated region decreases due to decreased light penetration (80 ppm, 48.20%, and 100 ppm, 42.81%) (the concentration of ppm is equal to mg/L). However, for diluted (low-colored) solutions, the degradation rate is commensurate to the ARS concentration (40 ppm, 68.89% and 20 ppm, 84.21%), as shown in table 4. The decomposition rate can almost reach the maximum [54]. This can be demonstrated by the actuality that when dye molecules occupy all catalyst sites, stabilization is observed with a fairly constant decomposition rate, followed by saturation and reduction in photoactivity. Coloring of solutions also represents a decrease in photosynthetic activity [55].

Hayder Khudhair Khattar, "Synthesis and Characterization SnO2/ZnO Ratio 1:1.25 Nanocomposite by Electrochemical Technique and Evaluated by Degradation of Alizarin Red S dye," *International Research Journal of Pharmacy and Medical Sciences (IRJPMS)*, Volume 9, Issue 1, pp. 6-16, 2025.

International Research Journal of Pharmacy and Medical Sciences
ISSN (Online): 2581-3277

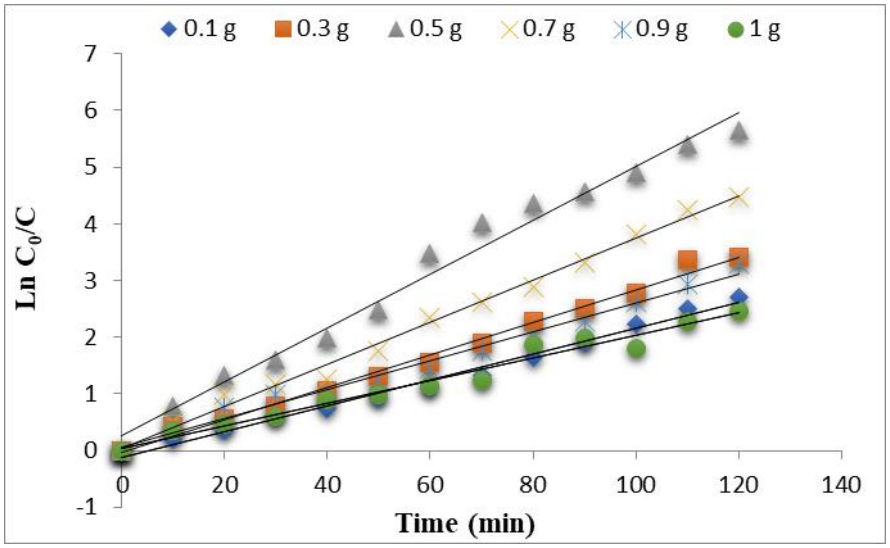

Figure 8. Change in photodegradation ratio with change in the weight of the catalyst, ARS %PDE (84.9%) is gained with a cata lyst dose of 0.5 g, rate constsnt k = 3.10×10^{-4}.

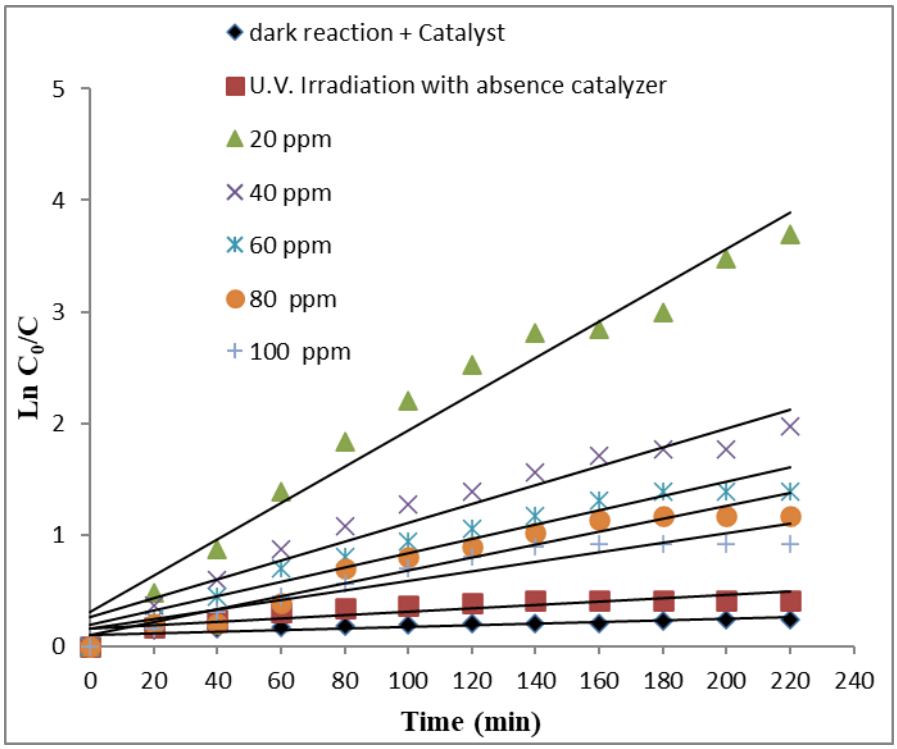

Figure 9. Effectiveness of the adsorption dark reaction for the nanocomposite (PDE=16.21, k = 0.43×10^{-4} sec^{-1}), the effectiveness of photocatalysis in the absence of the catalyst (PDE = 28.22%, k = 0.79×10^{-4} sec^{-1}), effectiveness of photocatalysis depending on the concentration, maximum value 20 ppm (PDE=84.21%, k=3.31×10^{-4} sec^{-1}).

TABLE 4. Values of photodegradation efficiency %PDE and rate constant (k) at different concentrations of the Alizarin Red S (ARS) dye

ppm	% PDE	k sec^{-1}
20	84.21	3.31×10^{-4}
40	68.89	2.01×10^{-4}
60	56.26	1.57×10^{-4}
80	48.20	1.18×10^{-4}
100	42.81	1.15×10^{-4}
U.V	28.22	0.79×10^{-4}
dark reaction	16.21	0.43×10^{-4}

Generating photons to decompose water pollutants is one of the most energy-intensive stages of treatment unit operation. In this context, photocatalysis contributes significantly to reducing water treatment costs. Therefore, ultraviolet light can be used as an effective energy source. The figure exhibits the degradation rate of ARS dye down to 250 W and UV irradiation and shows the degradation behavior in the dark. The kinetics of alizarin red S (ARS) degradation was studied based on the products published in the literature

Hayder Khudhair Khattar, "Synthesis and Characterization SnO2/ZnO Ratio 1:1.25 Nanocomposite by Electrochemical Technique and Evaluated by Degradation of Alizarin Red S dye," *International Research Journal of Pharmacy and Medical Sciences (IRJPMS)*, Volume 9, Issue 1, pp. 6-16, 2025.

[52, 54]. In more studies, the degradation of organic molecules to ARS is qualified as following the first-order kinetic model.

$$R = 100(C_0 - C_t)/C_0 \quad (1)$$

Where C_0 and C_t they are the initial concentration and the concentration at time t

$$r = \frac{dC}{dt} = k_{app}C_0 \quad (2)$$

Refer to *r* as the photocatalytic degradation velocity, k_{app} as the apparent degradation constant (min^{-1}), C_0 as the dye solution concentration (mg/L), and *t* is the irradiation time (min). Integrating this equation (in the limits $C = C_0$ at $t = 0$) leads to the following equation: The Langmuir-Hinshelwood model is described as pseudo-first order when the contaminant concentration is low and the adsorption process on the catalyst surface is in a quasi-steady state, resulting in the reaction rate being linearly proportional to the contaminant concentration in the solution [56].

$$\ln C_0/C = k_{app}t \quad (3)$$

Effect of Temperature on the Photodegradation of Alizarin Red S (ARS) Dye

The impact of temperature on the photodegradation of Alizarin Red S dye was calculated over a temperature range of 298–338 K, using an initial dye concentration of 20 ppm and a catalyst mass of 0.5 g of SnO_2/ZnO ratio (1:1.25) nanocomposites at pH = 9 and under 250 W UV light radiation. The results are appears in Figure 10., where the photodegradation rate constant $k = 8.3\times10^{-4}$ s^{-1} was recorded, and the photodegradation efficiency (PDE) reached approximately 86.11%. From the results, we notice that the Alizarin Red S dye is not significantly affected by an increase in temperature, and according to Arrhenius' law, the rate of chemical reactions changes with temperature according to the relationship.

$$k = Ae^{-Ea/RT} \quad (4)$$

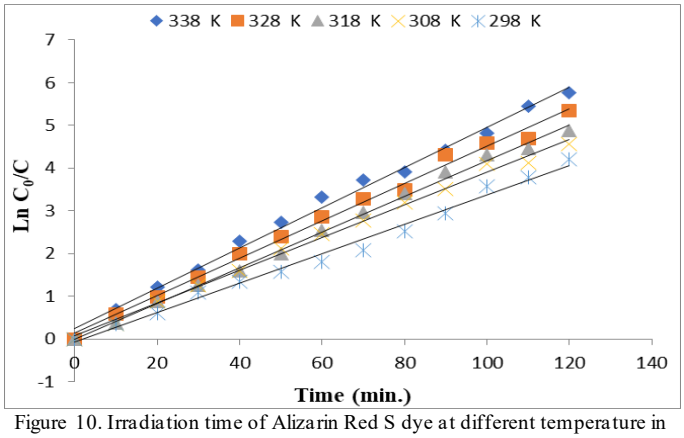

Figure 10. Irradiation time of Alizarin Red S dye at different temperature in presence SnO_2/ZnO ratio (1:1.25) nanocomposites, Photodegradation reaction, PDE=86.11%, Rate constant, $k = 8.3\times10^{-4}$ sec^{-1}.

The activation energy (E_a) of the thermal reaction can be calculated based on the straight-line equation derived from the Arrhenius equation. The graph representing the relationship between Ln k on the (y) axis and 1/T on the (x) axis is shown in Figure 11. Through the equation of a straight line, the slope of the curve can be determined, which is expressed by E_a/R, which equals E_a = 8.95 kJ mol^{-1} as shown in Figure 13. The entropy of activation ΔS^* was calculated from the same data. The activation entropy (ΔS^*) can also be estimated, which provides an indication of the degree of order or randomness in the transition state during the photolysis process. K_{338}, ΔS^*=-0.191 kJ mol^{-1} was calculated from equation 5 [57]:

$$\ln A = \ln K_B\, T/h + \frac{\Delta S^*}{R} \quad (5)$$

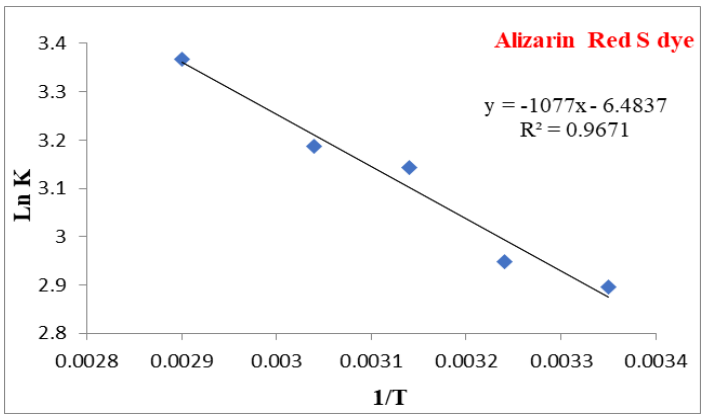

Figure 11. Arrhenius plot by using SnO_2/ZnO ratio (1:1.25) nanocomposites, as catalyst with Alizarin Red S dye at different temperature.

The Enthalpy of activation (K_{338}, ΔH^* = 6.144 kJ mol^{-1}) was calculated from equation:

$$\Delta H^* = Ea - RT \quad (6)$$

The free energy of activation (K_{338}, ΔG^* = 70.70 kJ mol^{-1}) was calculated from equation:

$$\Delta G^* = \Delta H^* - T\Delta S^* \quad (7)$$

The activation energy (E_a) for photodegradation and decolorization of ARS dye solution using a SnO_2/ZnO ratio (1:1.25) nanocomposite catalyst was calculated to be 8.95 kJ mol^{-1}. The very low activation energy value indicates that the photocatalytic reaction is weakly dependent on temperature, which can be explained by the photocatalytic activation mechanism [58]. Thermodynamic calculations of ARS dye decomposition showed that a positive ΔH^* value signals that the reaction is endothermic, while a positive ΔG^* value indicates that the reaction is non-spontaneous under the current experimental conditions [59]. This can be explained by the formation of a surface active phase characterized by high solubility, arising between the dye molecules and the generated hydroxyl radicals (•OH), which is also supported by the presence of negative activation entropy ($\Delta S^* < 0$) [60]. This negative value indicates that the intermediate formed is more ordered than the reactants. In the first stage, this medium is relatively unstable; however, the decomposition of the reactants into products proceeds remarkably quickly under the experimental conditions used, reflecting the high efficiency of the photocatalytic system based on SnO_2/ZnO, with a ratio of 1:1.25. The photodegradation mechanism of our nanocomposite starts when the light from the source is absorbed by the ZnO/Al_2O_3 layer [61], and the excitation electrons shift from the valence band to the conduction band. The transferred electrons minimize oxygen molecules to form superoxide anions (O_2^-), while holes oxidize water or hydroxide ions to generate hydroxyl radicals (•OH). These

Hayder Khudhair Khattar, "Synthesis and Characterization SnO2/ZnO Ratio 1:1.25 Nanocomposite by Electrochemical Technique and Evaluated by Degradation of Alizarin Red S dye," *International Research Journal of Pharmacy and Medical Sciences (IRJPMS)*, Volume 9, Issue 1, pp. 6-16, 2025.

reactive species decompose organic pollutants such as ARS dye into minimal molecules such as CO_2 and H_2O.

IV. Conclusion

In this research, a SnO_2/ZnO nanocomposite with a ratio of 1:1.25 was prepared, and its structural, surface, and functional properties were elaborate, in increment to estimate its efficiency as a photocatalyst for the degradation of alizarin red S (ARS) dye. Structural techniques (XRD, FTIR, FESEM, HRTEM, and EDX) detect that the composite was homogeneous, free of contamination, A smooth, interconnected surface was found to have a uniform distribution of the elements zinc, tin, and oxygen. The average particle size estimated from TEM/XRD (~19 nm) promoted the presence of regular nanoparticles, with a clear crystalline structure that facilitates electron transfer and enhances photocatalytic activity. The photodegradation survey of ARS dye offer that the nanocomposite was highly efficient, obtain high color abstraction (>86%) under the optimized experimental conditions (initial dye concentration 20 ppm, catalyst dosage 0.5 g, pH = 9, and light intensity 250 W at a temperature of 338 K). The photodegradation rate was also shown to rely on operational factors such as pH, dye concentration, and catalyst dosage, with the alkaline environment being maximum effective in inducing efficient electron–hole pair split. Kinetic and thermodynamic accounts indicated that the activation energy is very low (Ea = 8.95 kJ mol^{-1}), and that the photocatalytic reaction is little temperature dependent, with a negative entropy ($\Delta S^* < 0$) indicating that the transition state is more ordered. Also, a positive ΔH^* indicates that the reaction is endothermic, and a positive ΔG^* indicates that the process is non-spontaneous under the experimental conditions, reflecting the importance of the formation of an active surface phase that facilitates the oxidation of the dye by hydroxyl radicals $^{\bullet}OH$ and superoxide ions (O_2^-). The results proved that the reaction behaves as a pseudo-first-order reaction, the Langmuir-Hinshelwood model. The results confirm that the SnO_2/ZnO nanocomposite performs as an efficient and sustainable photocatalyst for the elimination of organic pollutants from water, with distinguished performance in the photodegradation of ARS dyes, making it suitable for environmental and industrial applications in industrial wastewater treatment.

Reference

[1] Vautier M, Guillard C, Herrmann JM. Photocatalytic degradation of dyes in water: case study of indigo and of indigo carmine. J Catal 2001;201:46e59.
[2] Guillard C, Lachheb H, Houas A, Ksibi M, Elaloui E, Herrmann JM. Influence of chemical structure of dyes, of pH and of inorganic salts on their photocatalytic degradation by TiO2 comparison of the efficiency of powder and supported TiO2. J Photochem Photobiol Chem 2003;158:27e36.
[3] Elsellami L, Vocanson F, Dappozze F, Baudot R, Febvay G, Rey M, et al. Kinetics and initial photocatalytic pathway of tryptophan, important constituent of microorganisms. Appl Catal B Environ 2010;94:192e9.
[4] Lachheb H, Dappozze F, Houas A, Guillard C. Adsorption and photocatalytic degradation of cysteine in presence of TiO2. J Photochem Photobiol Chem 2012;246:1e7.
[5] Iqbal T, Khan MA, Mahmood H. Facile synthesis of ZnO nanosheets: structural, antibacterial and photocatalytic studies. Mater Lett 2018;224:59e63.
[6] Han W, Ren L, Qi X, Liu Y, Wei X, Huang Z, et al. Synthesis of CdS/ZnO/graphene composite with high-efficiency photoelectrochemical activities under solar radiation. Appl Surf Sci 2014;299:12e8.
[7] Chatterjee D, Dasgupta S. Visible light induced photocatalytic degradation of organic pollutants. J Photochem Photobiol C Photochem Rev 2005;6:186e205.
[8] Duta M, Perniu D, Duta A. Photocatalytic zinc oxide thin films obtained by surfactant assisted spray pyrolysis deposition. Appl Surf Sci 2014;306:80e8.
[9] Zhiyong Y, Ruiying Q, Huanrong L, Zhiyin W, Xiaohong M, Chaonan D. Preparation and photocatalytic activity of SnO2. Mater Lett 2016;170:25e30.
[10] Kalantari Bolaghi Z, Masoudpanah SM, Hasheminiasari M. Photocatalytic activity of ZnO/RGO composite synthesized by one-pot solution combustion method. Mater Res Bull 2019;115:191e5.
[11] Di Paola A, Garcı´a-L_opez E, Marcı` G, Palmisano L. A survey of photocatalytic materials for environmental remediation. J Hazard Mater 2012;211e212:3e29.
[12] Kalantari Bolaghi Z, Hasheminiasari M, Masoudpanah SM. Solution combustion synthesis of ZnO powders using mixture of fuels in closed system. Ceram Int 2018;44:12684e90.
[13] Pearton SJ, Norton DP, Ip K, Heo YW, Steiner T. Recent progress in processing and properties of ZnO. Superlattice Microst 2003;34:3e32.
[14] Kalantari Bolaghi Z, Masoudpanah SM, Hasheminiasari M. Photocatalytic properties of ZnO powders synthesized by conventional and microwave-assisted solution combustion method. J Sol Gel Sci Technol 2018;86:711e8.
[15] Saravanan R, Karthikeyan S, Gupta VK, Sekaran G, Narayanan V, Stephen A. Enhanced photocatalytic activity of ZnO/CuO nanocomposite for the degradation of textile dye on visible light illumination. Mater Sci Eng C 2013;33:91e8.
[16] Li B, Wang Y. Facile synthesis and photocatalytic activity of ZnOeCuO nanocomposite. Superlattice Microst 2010;47:615e23.
[17] Girish Kumar S, Koteswara Rao KSR. Comparison of modification strategies towards enhanced charge carrier separation and photocatalytic degradation activity of metal oxide semiconductors (TiO2, WO3 and ZnO). Appl Surf Sci 2017;391:124e48.
[18] Upadhyay GK, Rajput JK, Pathak TK, Kumar V, Purohit LP. Synthesis of ZnO:TiO2 nanocomposites for photocatalyst application in visible light. Vacuum 2019;160:154e63.
[19] Liao S, Donggen H, Yu D, Su Y, Yuan G. Preparation and characterization of ZnO/TiO2, SO42_/ZnO/TiO2 photocatalyst and their photocatalysis. J Photochem Photobiol Chem 2004;168:7e13.
[20] Li B, Wang Y. Synthesis, microstructure, and photocatalysis of ZnO/CdS nano heterostructure. J Phys Chem Solid 2011;72:1165e9.
[21] Xu L, Xian F, Zhang Y, Wang W, Qiu K, Xu J. Synthesis of ZnO-decorated SnO2 nanopowder with enhanced photocatalytic performance. Optik 2019;194:162965.
[22] Li S, Pan J, Li H, Liu Y, Ou W, Wang J, et al. The transparent SnO/ZnO quantum dots/SnO2 p-n junction towards the enhancement of photovoltaic conversion. Chem Eng J 2019;366:305e12.
[23] Chen S, Liu F, Xu M, Yan J, Zhang F, Zhao W, et al. Firstprinciples calculations and experimental investigation on SnO2@ZnO hetero-junction photocatalyst with enhanced photocatalytic performance. J Colloid Interface Sci 2019;553:613e21.
[24] Yan J, Xu P, Chen S, Wang G, Zhang F, Zhao W, et al. Construction of highly ordered ZnO microrod@SnO2 nanowire hetero-junction hybrid with a test-tube brush-like structure for high performance lithium-ion batteries: experimental and theoretical study. Electrochim Acta 2020;330:135312.
[25] Li JC, Hou XY, Cao Q. Effect of Zn/Sn ratio on structure and properties of ZnOeSnO2 nanocomposite films. J Alloys Compd 2014;611:219e24.
[26] Lee SH, Lee S, Woo K, Kim YJ, Bak SY, Han YJ, et al. Effects of thermal annealing time and molar ratio of channel layers on solution-processed ZnO/SnO2 thin-film transistors. Solid State Electron 2020;165:107765.
[27] G. Asab, E.A. Zereffa, T. Abdo Seghne, Synthesis of Silica-Coated Fe3 O4 Nanoparticles by Microemulsion Method: Characterization and

Hayder Khudhair Khattar, "Synthesis and Characterization SnO2/ZnO Ratio 1:1.25 Nanocomposite by Electrochemical Technique and Evaluated by Degradation of Alizarin Red S dye," *International Research Journal of Pharmacy and Medical Sciences (IRJPMS)*, Volume 9, Issue 1, pp. 6-16, 2025.

Evaluation of Antimicrobial Activity, Int. J. Biomater. 2020 (Mar. 2020) 1–11, https://doi.org/ 10.1155/2020/4783612.

[28]. PATEL, Gauravkumar H., et al. Sol-gel synthesis and thermal characterization of SnO2 nanoparticles. Physica B: Condensed Matter, 2021, 613: 412987.

[29] CRIVELLARO, Simone, et al. A system for the synthesis of nanoparticles by laser ablation in liquid that is remotely controlled with PC or smartphone. Review of Scientific Instruments, 2019, 90.3.

[30] KAFI, F. S. B., et al. Electrodeposited thin film SnO2 photoelectrode for PEC applications. 2024.

[31] V. Kumar, K. Singh, J. Sharma, A. Kumar, A. Vij and A. Thakur, *J. Mater. Sci. Mater. Electron.*, 28, 18849 (2017); https://doi.org/10.1007/s10854-017-7836-z

[32] Shiri, H. M., Ehsani, A., Behjatmanesh-Ardakani, R., & Hajghani, S.. Electrosynthesis of Y2O3 nanoparticles and its nanocomposite with POAP as high efficient electrode materials in energy storage device: surface, density of state and electrochemical investigation. *Solid State Ionics*, 2019, 338: 87-95.

[33] Das, I., Sagadevan, S., Chowdhury, Z. Z., & Hoque, M. E.. Development, optimization and characterization of a two step sol–gel synthesis route for ZnO/SnO2 nanocomposite. Journal of Materials Science: Materials in Electronics, 2018, 29.5: 4128-4135.

[34] S. Abbasi, S.M. Zebarjad, S.H. Noie Baghban and A. Youssefi, *Synth. React. Inorg. Met.-Org. Nano-Met. Chem.*, 45, 1539 (2015); https://doi.org/10.1080/15533174.2013.862820

[35] G.C. Lakshmi, S. Ananda, R. Somashekar and C. Ranganathaiah, *Int. J. Adv. Sci. Technol.*, 5, 221 (2012).

[36] K. Byrappa, A.K. Subramani, S. Ananda, K.M.L. Rai, R. Dinesh and M. Yoshimura, *Bull. Mater. Sci.*, 29, 433 (2006); https://doi.org/10.1007/BF02914073.

[37] YUSUF, Moruf Olalekan. Bond characterization in cementitious material binders using Fourier-transform infrared spectroscopy. *Applied Sciences*, 2023, 13.5: 3353.

[38] GUO, Xin, et al. Molecular association of adsorbed water with lignocellulosic materials examined by micro-FTIR spectroscopy. *International journal of biological macromolecules*, 2016, 83: 117-125.

[39] YANG, Yuying, et al. Zn-O-Sn covalency interface governs the intrinsic activity of the Zn2SnO4/SnO2 heterostructure for boosting hydrogen peroxide production. Applied Catalysis B: Environment and Energy, 2025, 361: 124625. .

[40] THABOTHANAYAKAM, Tharsika. *Synthesis and Characterization of Zinc Oxide and tin Oxide Based Nanostructures for Gas Sensing Applications*. University of Malaya (Malaysia), 2015.

[41] KARTHIK, T. V. K.; MARTINEZ, L.; AGARWAL, V. Porous silicon ZnO/SnO2 structures for CO2 detection. *Journal of alloys and Compounds*, 2018, 731: 853-863.

[42] LIU, Jiangyang, et al. Highly sensitive and low detection limit of ethanol gas sensor based on hollow ZnO/SnO2 spheres composite material. *Sensors and Actuators B: Chemical*, 2017, 245: 551-559.

[43] Rogé, V., Didierjean, J., Crêpellière, J., Arl, D., Michel, M., Fechete, I., & Lenoble, D.. Tuneable functionalization of glass fibre membranes with ZnO/SnO2 heterostructures for photocatalytic water treatment: effect of SnO2 coverage rate on the photocatalytic degradation of organics. *Catalysts*, 2020, 10.7: 733.

[44] Arumugam, P., Masan, S., Venkatachalam, R., Peulakumari, P., Deivasikamani, V., & Rajendran, R. SnO2 nanoparticle reformed their magnetic properties by the efficiency of dopant cobalt (Co) in (Tin) Sn sites. *Materials Today: Proceedings*, 2021, 45: 3370-3373.

[45] PARK, Jongyoon, et al. Graphene-based two-dimensional mesoporous materials: Synthesis and electrochemical energy storage applications. *Materials*, 2021, 14.10: 2597.

[46] TARIQUE, Walia Binte. Synthesis and characterization of Zno/Sno2 nanocomposite via a two step spray pyrolysis route. 2019.

[47] SHAIK, Khajamuswareen, et al. Comparative study of crystallite size from XRD and TEM results for pure and V2O5 doped CdO-FePO4 composite nanopowders. Physical Chemistry Research, 2023, 11.2: 241-251.

[48] JADHAV, H. V.; KHETRE, S. M.; BAMANE, S. R. Removal of alizarin red-S from aqueous solution by adsorption on nanocrystalline Cu0. 5Zn0. 5Ce3O5. 2011.

[49] S. K. Kansal, R. Lamba, S. K. Mehta, and A. Umar, *Mater. Lett*., 386, 106 (2013).

[50] Ma, W., Zhang, Y., Li, F., Kou, D., & Lutkenhaus, J. L.. Layer-by-layer assembly and electrochemical study of alizarin red s-based thin films. Polymers, 2019, 11.1: 165.

[51] NAZ, Misbah, et al. Elimination of dyes by catalytic reduction in the absence of light: A review. *Journal of Materials Science*, 2021, 56.28: 15572-15608.

[52] R. Murugan, V. J. Babu, M. M. Khin, et al., *Mater. Lett.*, 97, 47-51 (2013).

[53] Liu, J., Zhao, H., Wu, M., Van der Schueren, B., Li, Y., Deparis, O., & Su, B. L. Slow photons for photocatalysis and photovoltaics. *Advanced Materials*, 2017, 29.17: 1605349.

[54] Ma, D., Li, J., Liu, A., & Chen, C. Carbon gels-modified TiO2: Promising materials for photocatalysis applications. Materials, 2020, 13.7: 1734.

[55] CHIU, Yi-Hsuan, et al. Mechanistic insights into photodegradation of organic dyes using heterostructure photocatalysts. *Catalysts*, 2019, 9.5: 430.

[56] MENA, E.; REY, A.; BELTRÁN, F. J. TiO2 photocatalytic oxidation of a mixture of emerging contaminants: A kinetic study independent of radiation absorption based on the direct-indirect model. *Chemical Engineering Journal*, 2018, 339: 369-380.

[57] HOSAMANI, Mohan T.; AYACHIT, Narasimha H.; DESHPANDE, D. K. Activation energy (Δ G*), enthalpy (Δ H*), and entropy (Δ S*) of some indoles and certain of their binary mixtures. Journal of thermal analysis and calorimetry, 2012, 107.3: 1301-1306.

[58] NURLAELA, Ela, et al. Temperature dependence of electrocatalytic and photocatalytic oxygen evolution reaction rates using NiFe oxide. Acs Catalysis, 2016, 6.3: 1713-1722.

[59] KHANDELWAL, Renu, et al. Biosorption of arsenic (III) from aqueous solution using calcium alginate immobilized dead biomass of Acinetobacter sp. strain Sp2b. *Scientific Reports*, 2024, 14.1: 9972.

[60] KARTHIKEYAN, S.; BOOPATHY, R.; SEKARAN, G. In situ generation of hydroxyl radical by cobalt oxide supported porous carbon enhance removal of refractory organics in tannery dyeing wastewater. *Journal of Colloid and Interface Science*, 2015, 448: 163-174.

[61] NOSAKA, Yoshio; NOSAKA, Atsuko Y. Generation and detection of reactive oxygen species in photocatalysis. *Chemical reviews*, 2017, 117.17: 11302-11336.